Published in final edited form as:
J Immunol. 2013 July 1; 191(1): 448–455. doi:10.4049/jimmunol.1203061.

Role of high endothelial venule-expressed heparan sulfate in chemokine presentation and lymphocyte homing[1]

Koichiro Tsuboi[*], **Jotaro Hirakawa**[*], **Emiko Seki**[*], **Yasuyuki Imai**[*], **Yu Yamaguchi**[†], **Minoru Fukuda**[‡], and **Hiroto Kawashima**[*,2]

[*]Laboratory of Microbiology and Immunology, School of Pharmaceutical Sciences, University of Shizuoka, Shizuoka 422-8526, Japan

[†]Genetic Disease Program, Sanford Children's Health Research Center, Sanford-Burnham Medical Research Institute, La Jolla, California 92037, USA

[‡]Glycobiology Unit, Tumor Microenvironment Program, Cancer Center, Sanford-Burnham Medical Research Institute, La Jolla, California 92037, USA

Abstract

Lymphocyte homing to peripheral lymph nodes (PLNs) is mediated by multi-step interactions between lymphocytes and high endothelial venules (HEVs). Heparan sulfate (HS) has been implicated in the presentation of chemokines on the surface of HEVs during this process. However, it remains unclear whether this cell surface presentation is a prerequisite for lymphocyte homing. In this paper, we generated conditional knockout (cKO) mice lacking *Ext1*, which encodes a glycosyltransferase essential for HS synthesis, by crossing *Ext1*$^{flox/flox}$ mice with *GlcNAc6ST-2-Cre* transgenic mice expressing Cre recombinase in HEVs. Immunohistochemical studies indicated that HS expression was specifically eliminated in PLN HEVs but retained in other blood vessels in the cKO mice. The accumulation of a major secondary lymphoid tissue chemokine, CCL21, on HEVs was also abrogated without affecting *CCL21* mRNA levels, indicating that HS presents CCL21 on HEVs *in vivo*. Notably, a short-term lymphocyte homing assay indicated that lymphocyte homing to PLNs was diminished in the cKO mice by 30 to 40%. Consistent with this result, contact hypersensitivity responses were also diminished in the cKO mice. The residual lymphocyte homing to PLNs in the cKO mice was dependent on pertussis toxin-sensitive G_i protein signaling, in which lysophosphatidic acid-mediated signaling was partly involved. These results suggest that chemokine presentation by HS on the surface of HEVs facilitates but is not absolutely required for lymphocyte homing.

Introduction

Lymphocyte homing to secondary lymphoid organs, such as peripheral lymph nodes (PLNs)[3] and Peyer's patches (PPs), through specialized blood vessels known as high endothelial venules (HEVs) is critical for immune surveillance (1–3). Lymphocyte homing

[1]This work was supported in part by PRESTO, JST (H.K.), a Grant-in-Aid for Scientific Research (B) from the Ministry of Education, Culture, Sports, Science and Technology, Japan (21390023 and 24390018, H.K.) and NIH grant P01CA71932 (M.F.).

Corresponding author: Hiroto Kawashima, Ph.D., Laboratory of Microbiology and Immunology, School of Pharmaceutical Sciences, University of Shizuoka, 52-1 Yada, Shizuoka 422-8526, Japan, Phone: +81-54-264-5710, Fax: +81-54-264-5715, kawashih@u-shizuoka-ken.ac.jp.

[3]Abbreviations used in this paper: PLNs, peripheral lymph nodes; PPs, Peyer's patches; HEVs, high endothelial venules; DKO, double knockout; GlcNAc6ST, GlcNAc-6-*O*-sulfotransferase; HS, heparan sulfate; cKO, conditional knockout; WT, wild-type; PTX, pertussis toxin; BrP-LPA, [1-bromo-3(S)-hydroxy-4-(palmitoyloxy)butyl]phosphonate; HEC, high endothelial cell; MACS, magnetic-activated cell sorting; LPA, lysophosphatidic acid.

is achieved by sequential interactions between lymphocytes and HEVs as follows (4): (i) lymphocyte rolling mediated by the interaction between L-selectin and its carbohydrate ligands, (ii) activation of lymphocytes by chemokines, (iii) integrin-mediated firm attachment of lymphocytes to HEVs, and (iv) transmigration.

Studies using glycan-synthesizing enzyme-deficient mice, such as fucosyltransferase-IV and -VII double knockouts (DKO) (5), GlcNAc-6-*O*-sulfotransferase (GlcNAc6ST)-1 and -2 DKOs (6, 7), and the recently reported sialyltransferase ST3Gal-IV and ST3Gal-VI DKOs (8), have demonstrated the essential role of an HEV-specific sulfated glycan, 6-sulfo sialyl Lewis X (Sialic acidα2-3Galβ1-4[Fucα1-3(sulfo-6)]GlcNAcβ1-R), in the initial step of these sequential interactions. The activation of lymphocytes by chemokines plays an essential role during the second step. In particular, studies using *plt* mice (9, 10) that lack secondary lymphoid-tissue chemokines, CCL21 and CCL19, and mice that lack their chemokine receptor, CCR7 (11), revealed a major role for these chemokines in lymphocyte homing to PLNs. A more recent study indicated that efficient lymphocyte homing could be observed in *Ccl19*-deficient mice (12), suggesting that CCL21 plays a dominant role in lymphocyte homing. Heparan sulfate (HS), another HEV-expressed sulfated glycan, has been implicated in the presentation of chemokines on the surface of HEVs and blood vessels at the site of inflammation (13–15). However, it remains unclear whether chemokine presentation by HEV-expressed HS is a prerequisite for lymphocyte homing.

The elongation of the HS backbone is catalyzed by the action of GlcA/GlcNAc copolymerases composed of Ext1 and Ext2 hetero-oligomers that elongate the nascent chain by adding alternating GlcA and GlcNAc residues (16). Systemic Ext1 knockout mice are almost completely deficient in HS synthesis and are embryonic lethal (17). Recently, a conditional deletion of Ext1 in a *Tek*-dependent and inducible manner succeeded in the generation of live animals that lack HS in the pan-endothelial cells. These mice demonstrated the function of HS in lymphocyte homing (18). However, the HS in all types of blood and lymphatic vessels was eliminated in those animals, which may have affected lymphocyte homing. In addition, Wang *et al.* reported that a pan-endothelial cell-specific conditional deletion of *N*-acetyl glucosamine *N*-deacetylase-*N*-sulfotransferase-1, which is required for *N*-sulfation of HS chains, caused a reduction of L-selectin- and chemokine-mediated neutrophil trafficking during the inflammatory responses (19). However, they did not report any physiological lymphocyte homing to the PLNs in the mutant animals.

We previously generated *GlcNAc6ST-2-Cre* transgenic mice expressing the Cre recombinase under the control of the regulatory elements of the gene for the HEV-restricted sulfotransferase gene, GlcNAc6ST-2, also known as high endothelial cell GlcNAc6ST or L-selectin ligand sulfotransferase (20). The expression of the Cre recombinase was restricted to the HEVs in the PLNs among all the blood vessels examined in the transgenic mice. In this study, we generated *Ext1* conditional knockout (cKO) mice by crossing the *GlcNAc6ST-2-Cre* transgenic mice with the $Ext1^{flox/flox}$ mice to determine the role of HEV-expressed HS in lymphocyte homing.

Materials and Methods

Mice

GlcNAc6ST-2-Cre transgenic mice (20) were crossed with $Ext1^{flox/flox}$ mice (21), and the male and female $GlcNAc6ST\text{-}2\text{-}Cre^{+/-}/Ext1^{flox/+}$ offspring were crossed to obtain the $GlcNAc6ST\text{-}2\text{-}Cre^{+/+}/Ext1^{flox/flox}$ male and $GlcNAc6ST\text{-}2\text{-}Cre^{+/-}/Ext1^{flox/flox}$ female mice. Thereafter, the $GlcNAc6ST\text{-}2\text{-}Cre^{+/+}/Ext1^{flox/flox}$ male and $GlcNAc6ST\text{-}2\text{-}Cre^{+/-}/Ext1^{flox/flox}$ female mice were further crossed, and the $GlcNAc6ST\text{-}2\text{-}Cre^{+/+}/Ext1^{flox/flox}$ and $GlcNAc6ST\text{-}2\text{-}Cre^{+/-}/Ext1^{flox/flox}$ offspring were used as the cKO mice. The

Ext1$^{flox/flox}$ mice were used as the wild-type (WT) controls throughout the study. The genomic DNA was isolated from the mouse tails and was used for PCR genotyping. All animal studies were performed in accordance with the guidelines of the Animal Research Committee of the University of Shizuoka.

Immunofluorescence

Frozen sections (7–μm thick) were fixed with ice-cold acetone and incubated with PBS containing 3% BSA (Sigma-Aldrich). To detect the HS in the PLNs, the sections were incubated with a mixture of 2.5 μg/ml biotinylated MECA-79 (Biolegend), 2.5 μg/ml Alexa Fluor 488-labeled rat anti-mouse CD31 mAb (MEC13.3, Biolegend), and 2.5 μg/ml mouse anti-HS mAb (10E4, mouse IgM, Seikagaku) that was fluorescently labeled with Alexa Fluor 594 carboxylic acid, succinimidyl ester (Invitrogen), followed by 2.5 μg/ml streptavidin-Alexa Fluor 405 (Invitrogen). To detect the HS in the PPs, the sections were incubated with 2.5 μg/ml MECA-367 (BD) that was fluorescently labeled with DyLight 488 NHS ester (Thermo Scientific) and 2.5 μg/ml Alexa Fluor 594-labeled 10E4. To detect the HS in the other tissues, the sections were incubated with a mixture of 5 μg/ml Alexa Fluor 488-labeled MEC13.3 and 2.5 μg/ml 10E4, followed by 1.0 μg/ml Alexa Fluor 594-labeled goat anti-mouse IgM (Invitrogen). To detect the CCL21 in the PLN HEVs, the sections were incubated with 10 μg/ml biotinylated-rabbit anti-mouse CCL21 (PeproTech) and 2.5 μg/ml MECA-79 (BD) that was fluorescently labeled with DyLight 488 NHS ester, followed by 1.0 μg/ml Alexa Fluor 594-conjugated streptavidin (Invitrogen). To detect other chemokines in the PLN HEVs, the sections were incubated with 10 μg/ml goat anti-mouse CCL19 (R&D) or 10 μg/ml goat anti-mouse CXCL13 (M-17, Santa Cruz Biotechnology) and 2.5 μg/ml DyLight 488-labeled MECA-79, followed by 1.0 μg/ml biotinylated donkey anti-goat IgG (Jackson ImmunoResearch Laboratories) and 1.0 μg/ml Alexa Fluor 594-conjugated streptavidin. After staining, the sections were mounted with Fluoromount (Diagnostic BioSystems). All images were obtained and analyzed with a BZ-9000 fluorescence microscope (KEYENCE).

Heparinase digestion and detection of CCL21 on the luminal surface of HEVs

Mice were injected intravenously with a mixture of *Bacteroides* heparinase I, heparinase II and heparinase III (New England BioLabs; heparinase I, heparinase II and heparinase III at a concentration of 75, 75 and 15 mU/g mouse body weight, respectively) in PBS. Four hours after the injection, the mice were injected intravenously with biotinylated-rabbit anti-mouse CCL21 (0.2 μg/g mouse body weight; PeproTech). Thirty minutes after the injection of the labeled antibody, PLNs were collected from each mouse, embedded in OCT compound (Sakura Finetek), frozen and stored at −80 °C. Frozen sections of the PLNs (10–μm thick) were fixed with PBS containing 1.75% formaldehyde (Kanto Chemical Co., Inc.) and incubated with PBS containing 3% BSA. The sections were incubated with a mixture of 2.5 μg/ml DyLight 488-labeled MECA-79 and 0.5 μg/ml Alexa Fluor 594-conjugated streptavidin. After staining, the sections were mounted with Fluoromount and analyzed with a BZ-9000 fluorescence microscope as described above.

Lymphocyte homing assay

Lymphocyte homing was assayed as previously described (6, 22) with several modifications. Briefly, the lymphocytes that were prepared from the spleens and MLNs of the WT mice were labeled with 5.0 μM carboxyfluorescein diacetate succinimidyl ester (CFSE, Invitrogen) and injected intravenously into the WT and cKO mice (2.0×10^5 lymphocytes/g mouse body weight). In some experiments, the recipient mice were treated with a mixture of *Bacteroides* heparinase I, heparinase II and heparinase III as described above for 4 h or with unlabeled rabbit anti-mouse CCL21 (PeproTech; 1.2 μg/g mouse body weight) for 30 min before the injection of the CFSE-labeled lymphocytes. In additional experiments, CFSE-

labeled lymphocytes (4×10^7 cells/ml) were treated with 100 ng/ml pertussis toxin (PTX) (List Biological Laboratories) or 50 μM [1-bromo-3(S)-hydroxy-4-(palmitoyloxy)butyl]phosphonate (BrP-LPA; Echelon Biosciences) in RPMI 1640 medium (Sigma-Aldrich) containing 10 mM HEPES and penicillin-streptomycin (Invitrogen) for 2 h at 37 °C, washed twice with RPMI 1640 medium containing 10% FBS (HyClone), 10 mM HEPES and penicillin-streptomycin, and resuspended in PBS (4×10^7 cells/ml) prior to intravenous injection into the recipient mice. Thirty min or 2 h after injection, the fraction of $CFSE^+$ cells in a cell suspension of the recipient lymphoid organs was determined by flow cytometry on a FACSCanto II flow cytometer (BD).

Flow cytometric analysis

Single-cell suspensions were prepared from the PLNs by passing the cells through a nylon mesh filter. The cells were incubated with 5 μg/ml anti-mouse CD16/32 (clone 93; Biolegend) to block the FcγII/III receptors. The cell suspension was then incubated with a combination of mAbs as follows: 4.0 μg/ml APC-conjugated anti-mouse CD3ε (2C11; eBioscience), 2.0 μg/ml R-phycoerythrin (PE)-conjugated anti-mouse CD45R/B220 (RA3-6B2; Biolegend), 1.25 μg/ml FITC-conjugated anti-mouse CD4 (RM4-5; eBioscience) and 2.5 μg/ml PE-Cy7-conjugated anti-mouse CD8 (53–6.7; Biolegend). The data were acquired by flow cytometry on a FACSCanto II flow cytometer and analyzed with the FACS Diva software (BD).

Purification of PLN high endothelial cells (HECs) from WT and cKO mice

Freshly isolated PLNs from the WT and cKO mice were minced with glass slides and incubated in RPMI 1640 containing 10% FBS, 10 mM HEPES, 1 mg/ml collagenase A (Roche), 0.5 mg/ml dispase (Invitrogen) and 10 U/ml DNase I (Roche) for 60 min at 37°C with gentle shaking. After centrifugation, the cells were resuspended in PBS containing 0.01% trypsin (Invitrogen) and 1 mM EDTA and incubated for 5 min at 37 °C. RPMI 1640 medium containing 10% FBS and 10 mM HEPES was added to terminate the trypsin digestion, and the cell suspension was passed through a 70-μm cell strainer (BD). The cells were incubated with 10 μg/ml MECA-79 (BD), followed by 10 μg/ml biotinylated mouse anti-rat IgM mAb (G53-238; BD). After washing with PBS containing 0.2% BSA, the cells were incubated with streptavidin-microbeads (1:10 dilution; Miltenyi Biotec) and 10 μg/ml streptavidin-conjugated Alexa Fluor 647 (Invitrogen). After washing, the MECA-79^+ HECs were purified using the MS column in the Mini magnetic-activated cell sorting (MACS) kit according to the manufacturer's protocol (Miltenyi Biotec). The HEC purities were determined by flow cytometry on a FACSCanto II flow cytometer. The total RNA was purified from the HECs and used for real-time quantitative PCR.

Real-time quantitative RT-PCR

The total RNA was extracted from the PLN HECs from the WT and cKO mice using the RNAspin Mini kit (GE Healthcare). The cDNA was synthesized using the PrimeScript RT-PCR kit (TaKaRa) and was subjected to real-time quantitative PCR using the SYBR Premix Ex Taq II (Tli RNase H Plus, TaKaRa). The expression of each mRNA was normalized to the expression of β-actin with the ΔΔCt method according to the manufacturer's instructions (TaKaRa Thermal Cycler Dice TP870). The primer sets used were as follows: β-actin, 5'-CATCCGTAAAGACCTCTATGCCAAC-3' and 5'-ATGGAGCCACCGATCCACA-3'; *Ext1*, 5'-GCCCTTTTGTTTTATTTTGG-3' and 5'-TCTTGCCTTTGTAGATGCTC-3'; *Ext2*, 5'-TCCAAGCTGCTGGTGGTCTG-3' and 5'-GCCTCTGTCTCGATTTCGTCGTA-3'; *Chst4*, 5'-GCATTATCCCAGCTACAGGATCAG-3' and 5'-TGGGAACCCAGGAACATCAG-3'; and *CCL21*, 5'-TGAGCTATGTGCAAACCCTGAGGA-3' and 5'-TGAGGGCTGTGTCTGTTCAGTTCT-3'.

PLN organ culture

PLNs, one each of the cervical, brachial, axillary, and inguinal lymph nodes, from the WT and cKO mice were cultured in 200 μl RPMI 1640 medium containing 10% FBS, 10 mM HEPES and penicillin-streptomycin at 37°C in a 5% CO_2 humidified incubator. After 24 h, the organ culture supernatants were collected, centrifuged to remove debris and used for ELISA.

ELISA for soluble CCL21

A 96-well ELISA plate (Corning) was coated with 0.5 μg/ml purified goat anti-mouse CCL21 antibody (anti-mouse 6Ckine antibody, R&D). After blocking with PBS containing 3% BSA, the recombinant mouse CCL21 (PeproTech), citrate plasma or the PLN organ culture supernatants were added to the wells and incubated for 1 h. After washing with PBS containing 0.05% Tween 20, 0.5 μg/ml biotinylated-rabbit anti-mouse CCL21 (PeproTech) was added to the wells and incubated for 1 h. After washing, alkaline phosphatase-conjugated streptavidin (1:2,000 dilution, Vector Laboratories) was added to the wells and incubated for 1 h. Finally, the BluePhos Microwell Phosphatase substrate (KPL) was added to the wells, and the optical density at 650 nm was measured using a 96-well spectrometer (SUNRISE Rainbow RC-R, TECAN). The value obtained with the RPMI 1640 medium containing 10% FBS, 10 mM HEPES and penicillin-streptomycin was subtracted from each measurement. The concentration of CCL21 in the PLN organ culture supernatants was estimated from a standard curve obtained with known amounts of recombinant mouse CCL21.

Contact hypersensitivity

Twenty five μl of 0.5% (v/v) DNFB (2,4-dinitrofluorobenzene, Wako) in acetone/olive oil (4:1) was applied onto the shaved forelegs of the mice on days 0 and 1. On day 5, the right ear was treated with 20 μl of 0.2% DNFB (10 μl on each side of the pinna), and the left ear was treated with vehicle. Ear swelling was measured with a Digimatic thickness gauge (Mitsutoyo, Japan) before and 24 h after treatment. After measurements were taken, some of the DNFB-treated ears were fixed with 10% formaldehyde in PBS and embedded in paraffin for hematoxylin-eosin staining. In parallel, some other DNFB-treated ears and draining lymph nodes were embedded in OTC compound, frozen and stored at −80 °C. Frozen sections were used for immunofluorescence as described above.

Statistical analysis

A Student's *t*-test or one-way ANOVA followed by a post hoc Dunnett's test was used to determine the statistical significance of the differences between experimental groups.

Results

Elimination of HS in PLN HEVs but not other blood vessels in cKO mice

To determine the expression of HS in the HEVs, the PLNs were collected from WT and cKO mice and subjected to immunofluorescence studies using the anti-HS mAb 10E4 and mAbs against pan-endothelial cells and HEVs. As shown in Figure 1A, the HS was strongly expressed in the HEVs expressing the pan-endothelial cell marker, CD31, and the PLN HEV marker, MECA-79, in the WT mice. By contrast, the HS was almost completely eliminated in the MECA-79^+ HEVs in the cKO mice. A quantitative analysis of the staining intensities of the HEVs with the anti-HS mAb indicated that 97% of the MECA-79^+ HEVs in the cKO mice expressed less than 10% HS compared with the average in the WT mice (Figure S1). The expression of HS in the $CD31^+$ blood vessels in the thymus, liver and kidney was unaffected in the cKO mice (Figure 1B). In addition, the expression of HS was also retained

in another type of HEV that was MECA-367 reactive (23) in the PPs of the cKO mice (Figure S2). These results indicate that the HS was almost completely eliminated in the MECA-79$^+$ HEVs but was retained in the other blood vessels of the cKO mice.

Diminished accumulation of CCL21 on PLN HEVs in cKO mice

CCL21 is a major secondary lymphoid-tissue chemokine that plays a critical role in lymphocyte homing (9–11). Notably, CCL21 can interact with various glycosaminoglycans, including HS, through its C-terminal highly basic region (24). To evaluate the CCL21 protein expression on the HEVs, the PLN sections from WT and cKO mice were stained with an anti-CCL21 polyclonal antibody and MECA-79. As shown in Figure 2, the accumulation of the CCL21 protein on the PLN HEVs was clearly observed in the WT mice, whereas no such accumulation was observed in the cKO mice. The accumulation of the other lymphoid chemokines CCL19 and CXCL13 on HEVs was not detected, even in the WT mice (Figure S3).

One may argue that the lack of CCL21 protein accumulation in the PLN HEVs in the cKO mice could be due to the reduction of CCL21 mRNA. To clarify this issue, we next examined CCL21 mRNA expression in the HEVs. The PLN HECs were purified from the WT and cKO mice by MACS using MECA-79. The HEC purities obtained were 88 to 96% as determined by flow cytometry. The total mRNAs that were prepared from the HECs were then subjected to real-time quantitative RT-PCR analysis (Figure 3A). As expected, the expression of the mRNA for a HEV-specific gene, *Chst4* (encoding *GlcNAc6ST-2*), was detected at a comparable level in both the HEC preparations. By contrast, the expression of the *Ext1* mRNA was diminished by 84% in the cKO mice, whereas the mRNA expression of *Ext2* was unchanged. The expression of *CCL21* mRNA in the cKO mice was comparable to that in the WT mice, indicating that the accumulation of CCL21 protein but not *CCL21* mRNA was diminished in the cKO mice.

The possibility remained that the CCL21 protein production but not the CCL21 protein presentation by HS may have been diminished in the cKO mice. To examine this possibility, the presence of soluble CCL21 in the plasma and PLN culture supernatants from WT and cKO mice was determined by a sandwich ELISA using anti-CCL21 polyclonal antibodies. As shown in Figure 3B, comparable amounts of soluble CCL21 were detected in the plasma and PLN culture supernatants of the cKO and WT mice, excluding the possibility that the protein production of CCL21 was diminished in the cKO mice. Taken together, these results indicate that the HS presents CCL21 proteins on the HEVs.

Role of HS in lymphocyte homing to PLNs

To assess the role of HS in lymphocyte homing, we next performed a lymphocyte homing assay. As shown in Figures 4A and 4B, the lymphocyte homing to the PLNs at 30 min and 2 h was diminished in the cKO mice by 37% and 29%, respectively. The number of lymphocytes in the PLNs of the cKO mice was also partially diminished by 30% compared to the WT mice (Figure 4C). By contrast, lymphocyte homing to the PPs was not diminished in the cKO mice, which is presumably due to the presence of MECA-367$^+$ HEVs that retained HS expression. The ratio of CD3$^+$ T cells to B220$^+$ B cells in the PLNs and PPs was not significantly changed in the cKO mice (Table I). These results suggest that chemokine presentation by HS facilitates but is not absolutely required for lymphocyte homing.

To determine whether lymphocytes can attach to and transmigrate through HEVs even when HS is eliminated, we next performed immunofluorescence studies of the PLNs that were injected with fluorescently labeled lymphocytes 30 min prior to tissue dissection. As shown

in Figure 5A, some lymphocytes could attach to the HEVs and were undergoing the process of transendothelial migration even in the cKO mice lacking the HS on the HEVs. In addition, fluorescently labeled lymphocytes that most likely transmigrated from the adjacent HEV into the parenchyma of the PLNs were observed in the cKO mice (Figure 5A, arrowheads). To determine whether the migratory properties of the lymphocytes in the parenchyma of the PLNs were affected in the cKO mice, the distances between the HEVs and the fluorescently labeled lymphocytes were measured. No significant difference in the distance between the HEVs and labeled lymphocytes was found in the WT and cKO mice, although the percentage of lymphocytes within 20 μm from the HEVs was slightly lower in the cKO mice (Figure 5B). These results suggest that the HS does not significantly affect the lymphocyte migration in the PLN parenchyma after the lymphocytes enter the tissue.

Characterization of residual lymphocyte homing in cKO mice

The above-mentioned results suggest that HS facilitates but is not absolutely required for lymphocyte homing. To determine the molecular mechanisms underlying the residual lymphocyte homing observed in the cKO mice, we examined the effects of various treatments on HEVs and lymphocytes (Fig. 5C). To examine the possibility that an incomplete deletion of HS from the surface of HEVs in the cKO mice might account for the residual homing, we first examined the effects of an intravenous injection of a mixture of heparinase I, heparinase II and heparinase III, which degrades HS. As shown in Fig. 5D, the heparinase treatment of WT mice abrogated the luminal surface presentation of CCL21 on MECA-79$^+$ HEVs as assessed by the intravenous injection of an anti-CCL21 polyclonal antibody, similar to what was observed in untreated cKO mice. Under such conditions, lymphocyte homing to PLN in the WT mice was diminished to the level observed in the cKO mice, while lymphocyte homing in the cKO mice was not affected (Fig. 5C). These results indicate that residual HS on the HEVs of the cKO mice does not account for the residual homing in the cKO mice. To explore the possibility that a form of CCL21 not bound to HS might be involved in the residual homing, we next examined the effects of an anti-CCL21 blocking antibody. The antibody treatment inhibited lymphocyte homing in the WT mice but not in the cKO mice, suggesting that molecules other than CCL21 are involved in the residual homing in the cKO mice. In contrast, PTX treatment of the CFSE-labeled lymphocytes inhibited homing by 85 to 90% in both the WT and the cKO mice, indicating that the residual homing was dependent on signaling through the G_i family of the G-protein coupled receptors but was independent of HS or CCL21.

We next examined whether the CXCL12-mediated signaling pathway might account for the residual pertussis toxin-sensitive G_i protein signaling because it was reported that this chemokine plays an important role in lymphocyte homing to PLNs in *plt/plt* mice that lack CCL21 and CCL19 in lymph nodes (10, 25, 26). However, anti-CXCL12 polyclonal antibodies, an anti-CXCR4 monoclonal antibody and a specific inhibitor of CXCL12-mediated signaling, AMD3100, failed to inhibit lymphocyte homing in both WT and cKO mice (unpublished observation). Recently, it was also reported that the lysophospholipase D/autotaxin expressed in HEVs and the product of this enzyme LPA (lysophosphatidic acid) are involved in lymphocyte homing (27–29). We thus examined the effects of BrP-LPA, which acts as an autotaxin inhibitor and pan-LPA receptor antagonist, on the residual lymphocyte homing in the cKO mice. As shown in Fig. 5C, the homing of BrP-LPA-treated lymphocytes was significantly inhibited in both the WT and cKO mice. The BrP-LPA treatment of lymphocytes did not affect lymphocyte L-selectin expression or the chemotactic responses of the lymphocytes toward CCL21 (unpublished observation). Collectively, these results indicate that the residual lymphocyte homing to PLNs in the cKO mice was dependent on pertussis toxin-sensitive G_i protein signaling, in which LPA-mediated signaling is partly involved.

Role of HEV-expressed HS in contact hypersensitivity

We next examined contact hypersensitivity responses in the cKO mice. As shown in Figs. 6A and 6B, ear swelling was diminished in the cKO mice by 49% compared to the WT mice in association with a diminished leukocyte infiltration of the ear. HS was expressed normally in the blood vessels of the inflamed ear in the cKO mice, while the presence of HS was eliminated in the HEVs of the draining lymph nodes in those mice (Fig. 6C). Collectively, these results indicate that HEV-expressed HS facilitates contact hypersensitivity responses.

Discussion

In this study, we generated cKO mice that specifically lacked Ext1 in HEVs by using *GlcNAc6ST-2-Cre* transgenic mice (20). We found that HS expression was specifically eliminated in HEVs in the PLNs but retained in other blood vessels in the cKO mice (Fig. 1). The generation of these highly specific cKO mice allowed us to examine the role of HEV-expressed HS in lymphocyte homing.

The accumulation of a major secondary lymphoid tissue chemokine, CCL21, on HEVs was abrogated without affecting *CCL21* mRNA levels (Figs. 2 and 3), indicating that HS presents CCL21 on HEVs *in vivo*. These findings are consistent with a previous model that glycosaminoglycans can immobilize chemokines on the surface of endothelial cells to prevent their rapid dilution by blood flow (13). CCL21 can interact with not only HS but also chondroitin sulfate (CS) B and CS E *in vitro* (24, 30). However, the present study clearly showed that HS is the sole glycosaminoglycan involved in CCL21 presentation on the surface of HEVs.

Notably, a short-term lymphocyte homing assay indicated that lymphocyte homing to PLNs was partially diminished in the cKO mice (Fig. 4). This result suggests that chemokine presentation by HS on HEVs facilitates lymphocyte homing. This finding also raised the question of why only a “partial” inhibition was observed in the cKO mice. It has been reported that 6-sulfo sialyl Lewis X-mediated lymphocyte rolling on HEVs is increased with the conditional deletion of Ext1 in a *Tek*-dependent and inducible manner, possibly because of the loss of electrostatic repulsion by HS (18). In addition, another report showed that the degradation of HS on endothelial cells exposes previously hidden endothelial cell surface adhesion molecules, including ICAM-1 and VCAM-1, during experimental sepsis (31). Therefore, it is likely that HS can function both positively and negatively in lymphocyte homing and that the partial inhibition of lymphocyte homing observed in our cKO mice could be due to the sum of these effects. A lack of HS may result in an enhancement of lymphocyte rolling and the ICAM-1-mediated firm attachment of lymphocytes, which may partly explain why lymphocyte homing was only partially inhibited in the cKO mice.

It should be noted, however, that lymphocyte homing is achieved by a multi-step process and that the activation of lymphocytes is critical to bridging these processes (4). Because HS-immobilized CCL21 was eliminated in our cKO mice, we think it is likely that some other signaling molecules may have activated lymphocytes during the process of lymphocyte homing in these animals. In agreement with this hypothesis, we found that the residual homing of lymphocytes in cKO mice could be significantly inhibited by PTX, indicating that the residual homing was dependent on signal transduction through the G_i family of the G-protein coupled receptors (Fig. 5). Furthermore, we found that LPA was partly involved in the residual homing in the cKO mice, consistent with previous findings that HEV-expressed autotaxin and the autotaxin product LPA are involved in lymphocyte homing (27–29) and that LPA induces the integrin-dependent adhesion of splenic B cells to ICAM-1 through G_i and G_{12}/G_{13} family of G-proteins (32).

Almost equivalent amount of soluble CCL21 was detected in the plasma and PLN organ culture supernatants of the WT and cKO mice (Fig. 3), even though the accumulation of CCL21 protein on HEVs was abolished in the cKO mice, as determined by immunofluorescence studies (Fig. 2). These findings suggest that the majority of locally produced CCL21 proteins was secreted from HEVs into the circulation and that only a portion of CCL21 proteins was presented on the surface of HEVs. However, our result that an anti-CCL21 polyclonal antibody failed to inhibit residual lymphocyte homing in the cKO mice (Fig. 5) suggests that HS-immobilized CCL21 may play a dominant role in lymphocyte homing, although we cannot exclude the possibility that soluble chemokines might also be involved in lymphocyte homing.

We demonstrated that contact hypersensitivity responses were significantly blocked in our cKO mice (Fig. 6), indicating that HEV-expressed HS which is involved in homing of naïve lymphocytes to PLNs is critical for the contact hypersensitivity response. It is noteworthy that the extent of the inhibition of contact hypersensitivity responses in mice lacking Ext1 in a *Tek*-dependent and inducible manner (18) was more significant than that observed in our HEV-specific cKO mice. The blood vessels of the inflamed ear lacked HS in the *Tek*-dependent and inducible cKO mice, but these vessels had normal levels of HS in our cKO mice. Therefore, the data obtained from the two different strains of cKO mice together indicate that HS expressed not only in HEVs but also in the blood vessels at inflammatory sites is important for the contact hypersensitivity response.

Collectively, our results suggest that chemokine presentation by HS facilitates but is not a prerequisite for lymphocyte homing. A previous model indicated that chemokines are presented by glycosaminoglycans on the surface of endothelial cells to induce lymphocyte adhesion (13), and this theory has since been widely accepted. However, our study now suggests that this model of chemokine presentation and lymphocyte homing may need refinement and updating.

Supplementary Material

Refer to Web version on PubMed Central for supplementary material.

References

1. Butcher EC, Picker LJ. Lymphocyte homing and homeostasis. Science. 1996; 272:60–66. [PubMed: 8600538]
2. von Andrian UH, Mempel TR. Homing and cellular traffic in lymph nodes. Nat Rev Immunol. 2003; 3:867–878. [PubMed: 14668803]
3. Girard JP, Moussion C, Forster R. HEVs, lymphatics and homeostatic immune cell trafficking in lymph nodes. Nat Rev Immunol. 2012; 12:762–773. [PubMed: 23018291]
4. Springer TA. Traffic signals for lymphocyte recirculation and leukocyte emigration: the multistep paradigm. Cell. 1994; 76:301–314. [PubMed: 7507411]
5. Homeister JW, Thall AD, Petryniak B, Maly P, Rogers CE, Smith PL, Kelly RJ, Gersten KM, Askari SW, Cheng G, Smithson G, Marks RM, Misra AK, Hindsgaul O, von Andrian UH, Lowe JB. The α(1,3)fucosyltransferases FucT-IV and FucT-VII exert collaborative control over selectin-dependent leukocyte recruitment and lymphocyte homing. Immunity. 2001; 15:115–126. [PubMed: 11485743]
6. Kawashima H, Petryniak B, Hiraoka N, Mitoma J, Huckaby V, Nakayama J, Uchimura K, Kadomatsu K, Muramatsu T, Lowe JB, Fukuda M. *N*-acetylglucosamine-6-*O*-sulfotransferases 1 and 2 cooperatively control lymphocyte homing through L-selectin ligand biosynthesis in high endothelial venules. Nat Immunol. 2005; 6:1096–1104. [PubMed: 16227985]

7. Uchimura K, Gauguet JM, Singer MS, Tsay D, Kannagi R, Muramatsu T, von Andrian UH, Rosen SD. A major class of L-selectin ligands is eliminated in mice deficient in two sulfotransferases expressed in high endothelial venules. Nat Immunol. 2005; 6:1105–1113. [PubMed: 16227986]
8. Yang WH, Nussbaum C, Grewal PK, Marth JD, Sperandio M. Coordinated roles of ST3Gal-VI and ST3Gal-IV sialyltransferases in the synthesis of selectin ligands. Blood. 2012; 120:1015–1026. [PubMed: 22700726]
9. Gunn MD, Kyuwa S, Tam C, Kakiuchi T, Matsuzawa A, Williams LT, Nakano H. Mice lacking expression of secondary lymphoid organ chemokine have defects in lymphocyte homing and dendritic cell localization. J Exp Med. 1999; 189:451–460. [PubMed: 9927507]
10. Luther SA, Tang HL, Hyman PL, Farr AG, Cyster JG. Coexpression of the chemokines ELC and SLC by T zone stromal cells and deletion of the ELC gene in the *plt/plt* mouse. Proc Natl Acad Sci U S A. 2000; 97:12694–12699. [PubMed: 11070085]
11. Forster R, Schubel A, Breitfeld D, Kremmer E, Renner-Muller I, Wolf E, Lipp M. CCR7 coordinates the primary immune response by establishing functional microenvironments in secondary lymphoid organs. Cell. 1999; 99:23–33. [PubMed: 10520991]
12. Link A, Vogt TK, Favre S, Britschgi MR, Acha-Orbea H, Hinz B, Cyster JG, Luther SA. Fibroblastic reticular cells in lymph nodes regulate the homeostasis of naive T cells. Nat Immunol. 2007; 8:1255–1265. [PubMed: 17893676]
13. Tanaka Y, Adams DH, Hubscher S, Hirano H, Siebenlist U, Shaw S. T-cell adhesion induced by proteoglycan-immobilized cytokine MIP-1β. Nature. 1993; 361:79–82. [PubMed: 7678446]
14. Parish CR. The role of heparan sulphate in inflammation. Nat Rev Immunol. 2006; 6:633–643. [PubMed: 16917509]
15. Kawashima H. Roles of sulfated glycans in lymphocyte homing. Biol Pharm Bull. 2006; 29:2343–2349. [PubMed: 17142960]
16. McCormick C, Duncan G, Goutsos KT, Tufaro F. The putative tumor suppressors EXT1 and EXT2 form a stable complex that accumulates in the Golgi apparatus and catalyzes the synthesis of heparan sulfate. Proc Natl Acad Sci U S A. 2000; 97:668–673. [PubMed: 10639137]
17. Lin X, Wei G, Shi Z, Dryer L, Esko JD, Wells DE, Matzuk MM. Disruption of gastrulation and heparan sulfate biosynthesis in EXT1-deficient mice. Dev Biol. 2000; 224:299–311. [PubMed: 10926768]
18. Bao X, Moseman EA, Saito H, Petryniak B, Thiriot A, Hatakeyama S, Ito Y, Kawashima H, Yamaguchi Y, Lowe JB, von Andrian UH, Fukuda M. Endothelial heparan sulfate controls chemokine presentation in recruitment of lymphocytes and dendritic cells to lymph nodes. Immunity. 2010; 33:817–829. [PubMed: 21093315]
19. Wang L, Fuster M, Sriramarao P, Esko JD. Endothelial heparan sulfate deficiency impairs L-selectin- and chemokine-mediated neutrophil trafficking during inflammatory responses. Nat Immunol. 2005; 6:902–910. [PubMed: 16056228]
20. Kawashima H, Hirakawa J, Tobisawa Y, Fukuda M, Saga Y. Conditional gene targeting in mouse high endothelial venules. J Immunol. 2009; 182:5461–5468. [PubMed: 19380794]
21. Inatani M, Irie F, Plump AS, Tessier-Lavigne M, Yamaguchi Y. Mammalian brain morphogenesis and midline axon guidance require heparan sulfate. Science. 2003; 302:1044–1046. [PubMed: 14605369]
22. Hiraoka N, Kawashima H, Petryniak B, Nakayama J, Mitoma J, Marth JD, Lowe JB, Fukuda M. Core 2 branching β1,6-*N*-acetylglucosaminyltransferase and high endothelial venule-restricted sulfotransferase collaboratively control lymphocyte homing. J Biol Chem. 2004; 279:3058–3067. [PubMed: 14593101]
23. Nakache M, Berg EL, Streeter PR, Butcher EC. The mucosal vascular addressin is a tissue-specific endothelial cell adhesion molecule for circulating lymphocytes. Nature. 1989; 337:179–181. [PubMed: 2911352]
24. Hirose J, Kawashima H, Swope Willis M, Springer TA, Hasegawa H, Yoshie O, Miyasaka M. Chondroitin sulfate B exerts its inhibitory effect on secondary lymphoid tissue chemokine (SLC) by binding to the C-terminus of SLC. Biochim Biophys Acta. 2002; 1571:219–224. [PubMed: 12090936]

25. Okada T, Ngo VN, Ekland EH, Forster R, Lipp M, Littman DR, Cyster JG. Chemokine requirements for B cell entry to lymph nodes and Peyer's patches. J Exp Med. 2002; 196:65–75. [PubMed: 12093871]
26. Nakano H, Gunn MD. Gene duplications at the chemokine locus on mouse chromosome 4: multiple strain-specific haplotypes and the deletion of secondary lymphoid-organ chemokine and EBI-1 ligand chemokine genes in the *plt* mutation. J Immunol. 2001; 166:361–369. [PubMed: 11123313]
27. Kanda H, Newton R, Klein R, Morita Y, Gunn MD, Rosen SD. Autotaxin, an ectoenzyme that produces lysophosphatidic acid, promotes the entry of lymphocytes into secondary lymphoid organs. Nat Immunol. 2008; 9:415–423. [PubMed: 18327261]
28. Zhang Y, Chen YC, Krummel MF, Rosen SD. Autotaxin through lysophosphatidic acid stimulates polarization, motility, and transendothelial migration of naive T cells. J Immunol. 2012; 189:3914–3924. [PubMed: 22962684]
29. Bai Z, Cai L, Umemoto E, Takeda A, Tohya K, Komai Y, Veeraveedu PT, Hata E, Sugiura Y, Kubo A, Suematsu M, Hayasaka H, Okudaira S, Aoki J, Tanaka T, Albers HM, Ovaa H, Miyasaka M. Constitutive Lymphocyte Transmigration across the Basal Lamina of High Endothelial Venules Is Regulated by the Autotaxin/Lysophosphatidic Acid Axis. J Immunol. 2013; 190:2036–2048. [PubMed: 23365076]
30. Kawashima H, Atarashi K, Hirose M, Hirose J, Yamada S, Sugahara K, Miyasaka M. Oversulfated chondroitin/dermatan sulfates containing GlcAβ1/IdoAα1-3GalNAc(4,6-*O*-disulfate) interact with L- and P-selectin and chemokines. J Biol Chem. 2002; 277:12921–12930. [PubMed: 11821431]
31. Schmidt EP, Yang Y, Janssen WJ, Gandjeva A, Perez MJ, Barthel L, Zemans RL, Bowman JC, Koyanagi DE, Yunt ZX, Smith LP, Cheng SS, Overdier KH, Thompson KR, Geraci MW, Douglas IS, Pearse DB, Tuder RM. The pulmonary endothelial glycocalyx regulates neutrophil adhesion and lung injury during experimental sepsis. Nat Med. 2012; 18:1217–1223.
32. Rieken S, Herroeder S, Sassmann A, Wallenwein B, Moers A, Offermanns S, Wettschureck N. Lysophospholipids control integrin-dependent adhesion in splenic B cells through G_i and G_{12}/G_{13} family G-proteins but not through G_q/G_{11}. J Biol Chem. 2006; 281:36985–36992. [PubMed: 17023430]

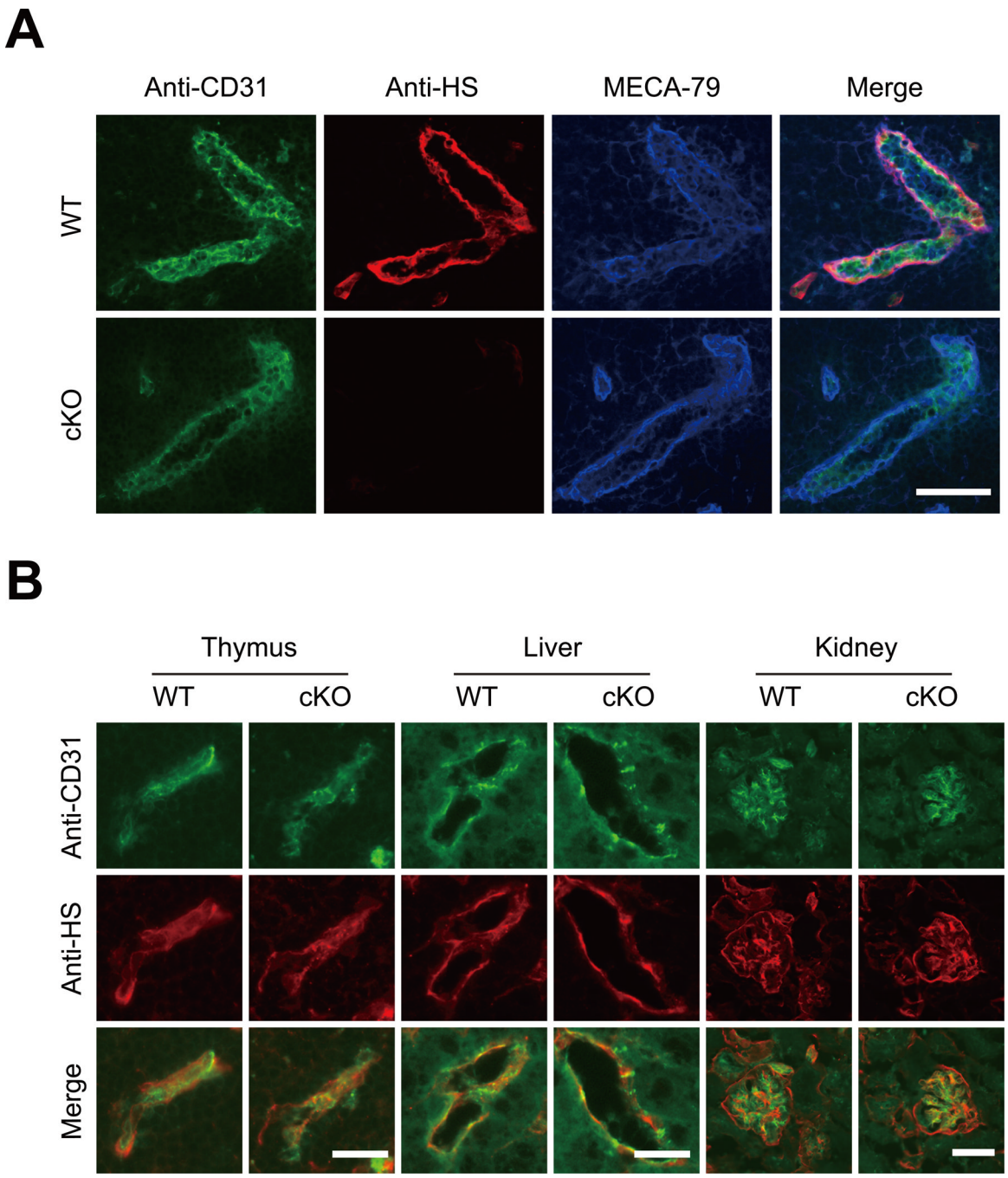

Figure 1. Expression of HS in PLN HEVs and other blood vessels

(A) Frozen sections of the PLNs from the WT and cKO mice were stained with an anti-CD31 mAb (*green*), anti-HS mAb (*red*) and MECA-79 (*blue*). Scale bar, 50 μm. **(B)** Frozen sections of the thymus, liver and kidney from the WT and cKO mice were stained with an anti-CD31 mAb (*green*) and anti-HS mAb (*red*). Scale bars: 20 μm for thymus and liver and 50 μm for kidney. The data are representative of three independent experiments.

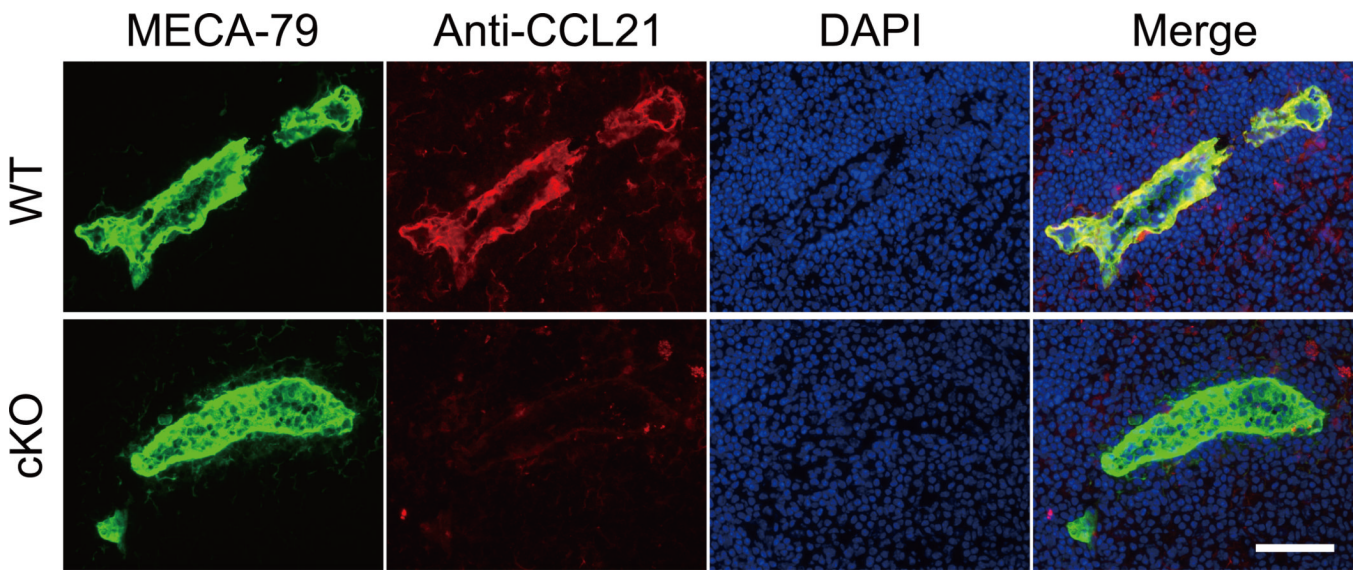

Figure 2. Diminished accumulation of CCL21 on PLN HEVs in cKO mice

Frozen sections of PLNs were stained with polyclonal antibodies against CCL21 (*red*) and MECA-79 (*green*). Nuclear staining was performed with DAPI (*blue*). Scale bar, 50 μm. The data are representative of three independent experiments.

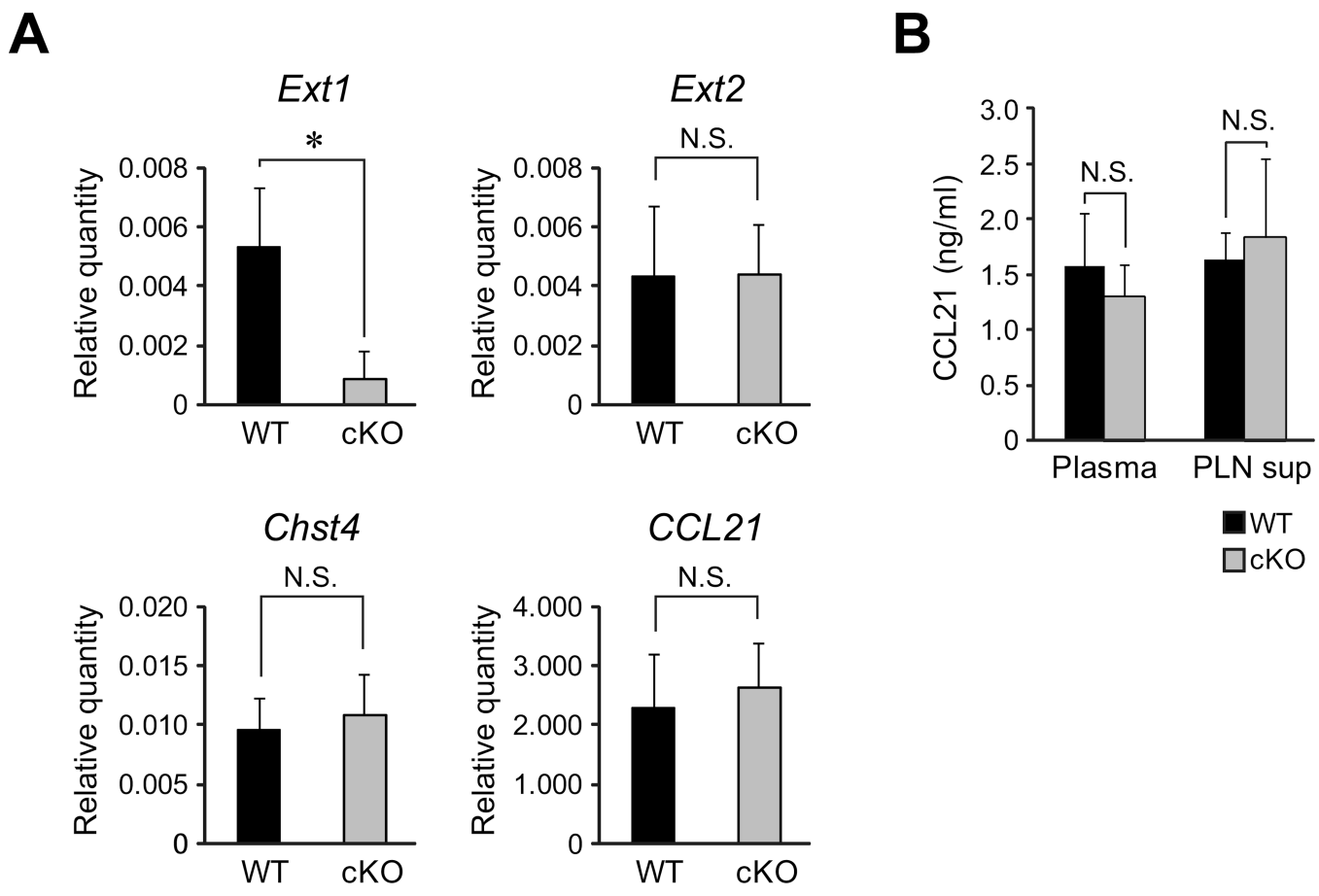

Figure 3. Real-time quantitative RT-PCR analysis and ELISA for CCL21

(A) Real-time RT-PCR analysis. The expression of the mRNAs for *Ext-1*, *Ext-2*, *Chst4* and *CCL21* were analyzed by real-time RT-PCR using the total RNA samples from the MECA-79$^+$ HECs from the WT and cKO mice. The relative quantity of each mRNA compared to the quantity of β-actin was determined by the ΔΔCt method. Each bar represents the mean ± SD. *, $P < 0.02$ versus the WT mice. *N.S.*, not significant. The data from three independent experiments were pooled ($n = 3$). **(B)** Detection of soluble chemokines in the citrate-plasma (*Plasma*) and PLN organ culture supernatant (*PLN sup*) from the WT and cKO mice by ELISA. Each bar represents the mean ± SD. *N.S.*, not significant. The data are representative of three independent experiments.

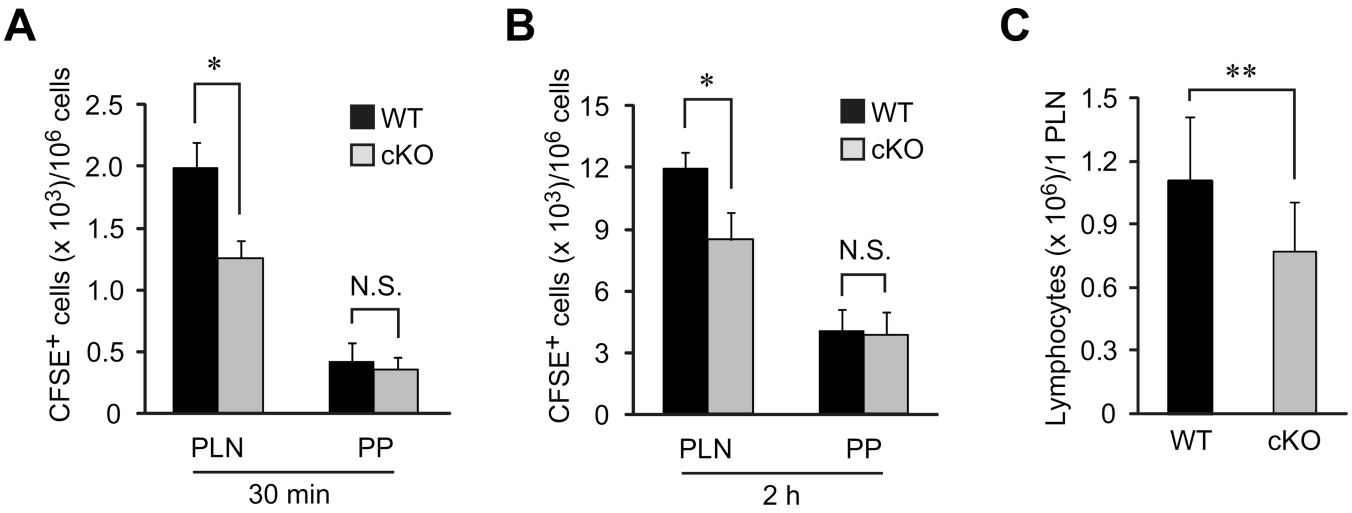

Figure 4. Partial reduction of lymphocyte homing to PLNs in cKO mice

(A, B) Lymphocytes labeled with CFSE were injected into the tail veins of WT and cKO mice. Thirty min **(A)** or 2 h **(B)** after injection, the fluorescent lymphocytes from the PLNs and PPs were quantified by flow cytometry. Four to five recipient mice were tested in each experiment. Each bar represents the mean ± SD. *, $P < 0.002$ versus the WT mice. *N.S.*, not significant. The data are representative of two independent experiments. **(C)** The lymphocytes recovered from the PLNs of the WT and cKO mice were counted, and the average number of lymphocytes per PLN was calculated. Each bar represents the mean ± SD. **, $P < 0.02$ versus the WT mice. The number of mice analyzed were as follows: $n = 14$ (WT) and $n = 13$ (cKO).

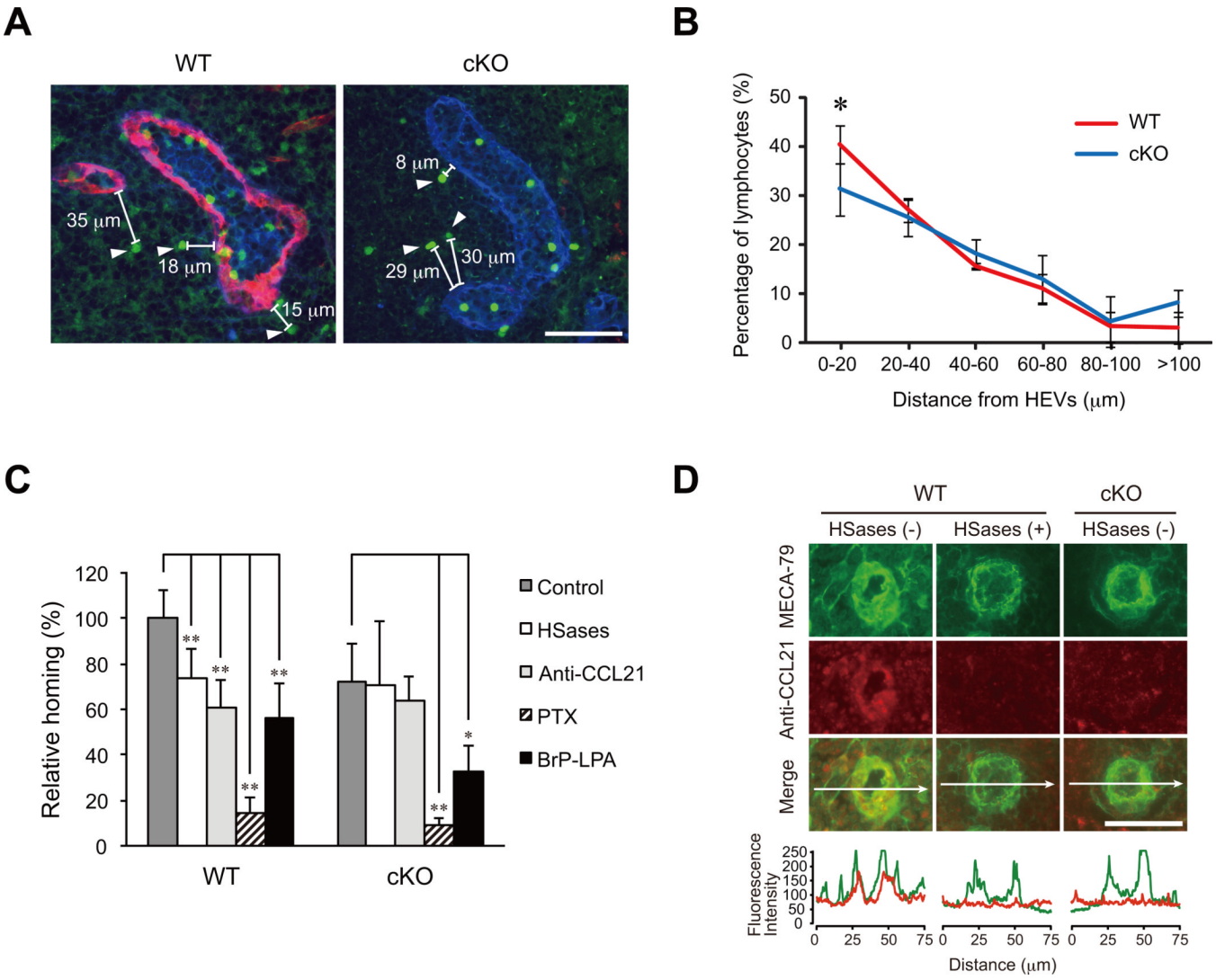

Figure 5. Characterization of residual lymphocyte homing in cKO mice

(A) A typical example of the transendothelial migration of CFSE-labeled lymphocytes into the parenchyma of the PLNs. The CFSE-labeled lymphocytes were injected 30 min prior to tissue dissection. The sections were stained with an anti-HS mAb (*red*) and MECA-79 (*blue*). The *arrowheads* denote the CFSE-labeled lymphocytes that have transmigrated from the adjacent HEV into the parenchyma of the PLNs. The distance between the transmigrated CFSE-labeled lymphocytes and the most adjacent HEVs was measured with the fluorescence microscope, BZ-9000. Scale bar, 50 μm. **(B)** The distribution of the distance between the CFSE-labeled lymphocytes and the PLN HEVs in the WT and cKO mice. The values represent the mean ± SD. *, $P < 0.05$ versus the WT mice ($n = 3$). The data are representative of two independent experiments. **(C)** Lymphocytes labeled with CFSE that had been treated with or without PTX or BrP-LPA were injected into the tail veins of WT or cKO mice that had been treated with or without a mixture of heparinase I, heparinase II and heparinase III (*HSases*) or anti-CCL21 polyclonal antibody (*Anti-CCL21*). Thirty min after injection, the fluorescent lymphocytes from the PLNs were quantified with flow cytometry. The relative amount of lymphocyte homing is shown as a percentage of that observed with the untreated control lymphocytes in WT mice, which is set as 100%. Three to five recipient mice were tested in each experimental group. Each bar represents the mean ± SD. *, $P <$

0.05; **, $P < 0.01$ versus the untreated control. **(D)** The detection of CCL21 on the luminal surface of HEVs. WT mice that had been treated with or without a mixture of heparinase I, heparinase II and heparinase III (*HSases*) or cKO mice were injected intravenously with biotinylated anti-CCL21 polyclonal antibody. Frozen sections of the PLNs from those mice were stained with DyLight 488-labeled MECA-79 and Alexa Fluor 594-conjugated streptavidin. The profile of the fluorescence intensity along the white arrow in each merged image is shown at the bottom. Note that the CCL21 accumulation (*red*) on HEVs was diminished in the HSase-treated WT mice and untreated cKO mice. Scale bar, 50 μm.

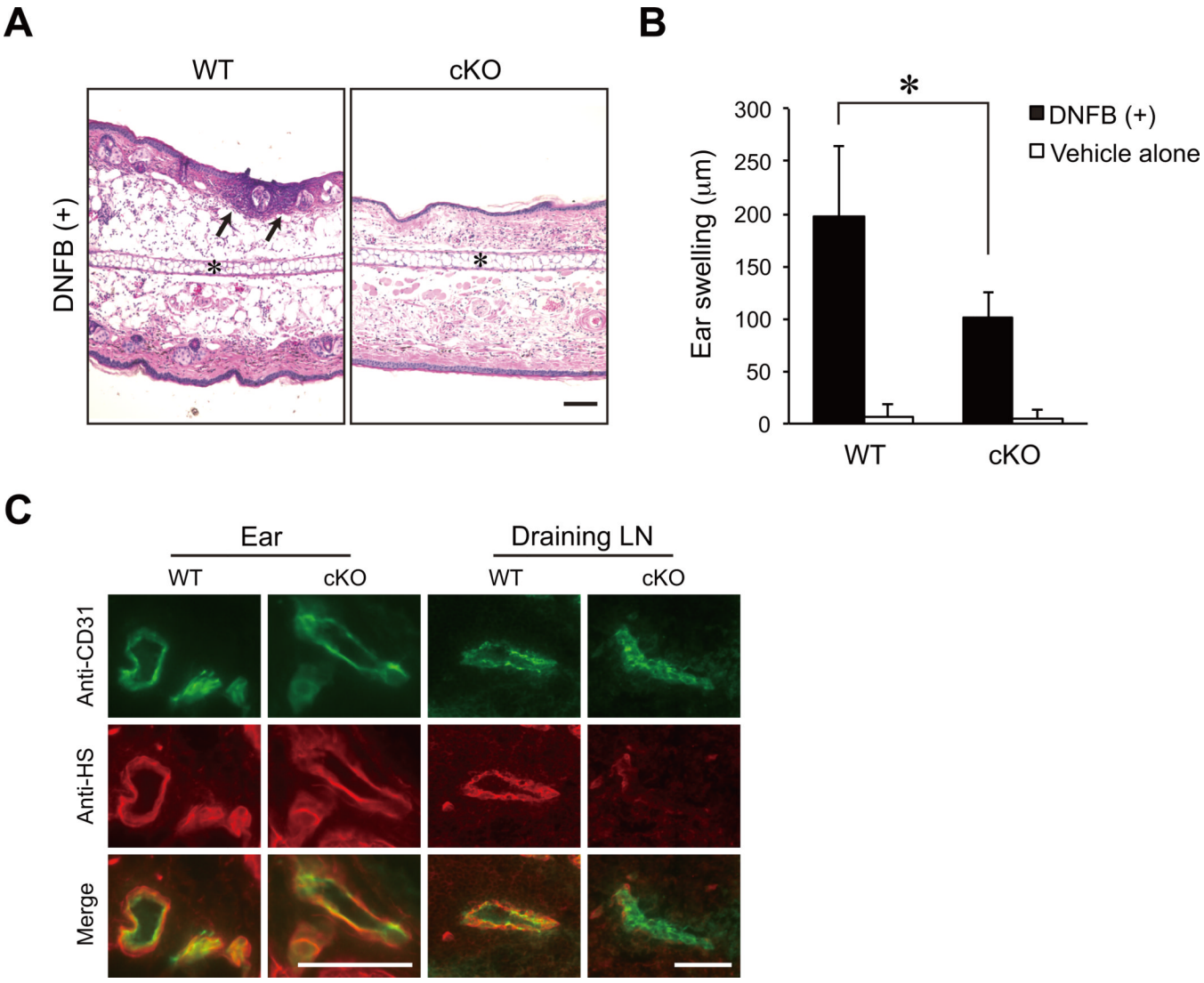

Figure 6. Diminished contact hypersensitivity responses in cKO mice

(A) Hematoxylin-eosin staining of ear sections 24 h after DNFB challenge on day 5. *, ear cartilage; arrows, recruited leukocytes. Scale bar, 100 μm. **(B)** Ear swelling 24 h after the challenge with DNFB or vehicle alone on day 5 in the WT and cKO mice (n = 5). *, $P < 0.01$ **(C)** Frozen sections of the DNFB-treated ear and draining lymph node (*Draining LN*) from the WT and cKO mice were stained with an anti-CD31 mAb (*green*) and an anti-HS mAb (*red*). Scale bars, 50 μm. The data are representative of two independent experiments.

Table I

Percentage of lymphocyte subpopulations in PLNs of WT and cKO mice.

	Cells in PLN (%)*		Cells in PP (%)	
	WT	**cKO**	**WT**	**cKO**
$CD3^+$	53.4 ± 5.8	52.0 ± 4.2	14.4 ± 1.1	14.6 ± 2.4
$CD3^+$ $CD4^+$	24.8 ± 3.5	25.9 ± 2.9	10.4 ± 0.8	9.6 ± 2.0
$CD3^+$ $CD8^+$	26.0 ± 2.5	23.3 ± 1.8	2.0 ± 0.3	2.0 ± 0.1
$B220^+$	38.2 ± 5.6	38.8 ± 4.4	78.4 ± 1.8	79.2 ± 2.1
Others	8.5 ± 1.7	9.2 ± 3.3	7.2 ± 1.3	6.2 ± 0.7

*The values represent the means ± SD of the cell percentages in the PLNs per mouse (n = 3).

**The data are representative of three independent experiments.